





Cite this: DOI: 10.1039/d5nr01345c

## Growth of highly uniform 2-inch MoS<sub>2</sub> wafers using liquid precursor spraying

Xin Lu, Jinxiu Liu, Ding Lu, Chunchi Zhang, Xika Zhang, Zhaokuan Wen, Chao Tan  and Zegao Wang \*

With the progress of study, MoS<sub>2</sub> has been proven to show excellent properties in electronics and optoelectronics, which promotes the fabrication of future novel integrated circuits and photodetectors. However, highly uniform wafer-scale growth is still in its early stage, especially regarding how to control the precursor and its distribution. Herein, we propose a new method, spraying the Mo precursor, which is proven to fabricate highly uniform 2-inch monolayer MoS<sub>2</sub> wafers. The Mo-precursor concentration and spray time are the key parameters, which have been systematically studied. The monolayer and bilayer coverage, Raman vibration, and PL emission properties are investigated. It was found that when the Mo-precursor concentration is 10 mg mL<sup>-1</sup> and spray time is 8 min, the as-grown MoS<sub>2</sub> wafer has the highest quality and electrical performance. By studying the electrical properties of transistor arrays, it was found that the MoS<sub>2</sub> transistors show slight vibration, the average ON/OFF ratio is  $1.21 \times 10^6$ , and the maximum carrier mobility is 13.39 cm<sup>2</sup> V<sup>-1</sup> s<sup>-1</sup> without further optimizing the device fabrication. These results directly indicate that the spray method could fabricate MoS<sub>2</sub> wafers with both high optical and electrical uniformity. Moreover, the influence of bilayer coverage on the optical and electrical properties is studied, which demonstrates that additional bilayer nucleation would increase the scattering centers and thus suppress the electrical performance. By this method, we have successfully grown more than 100 2-inch wafers with a stable process, which further proves its potential application in future MoS<sub>2</sub> electronics and integrated circuits.

Received 2nd April 2025,  
Accepted 16th August 2025

DOI: 10.1039/d5nr01345c

rsc.li/nanoscale

## Introduction

Two-dimensional materials have emerged as critical candidates for next-generation electronics due to their unique characteristics of atomic-scale thickness and modifiable band structures, which enable the fabrication of sub-nanometer narrow transistors and facilitate the construction of nanoelectronics for future post-Moore era.<sup>1–3</sup> Up to now, although the 2D family has many members, molybdenum disulfide (MoS<sub>2</sub>) has received the most investigations, including its growth and application in electronic devices and optoelectronic devices.<sup>4–6</sup> A MoS<sub>2</sub>-based integrated circuit has become more and more urgent. Recently, many industries have also paid attention to MoS<sub>2</sub>, such as TMC, Samsung, *etc.* After more than ten years, many novel devices have been proposed and proven; however, controlled wafer-scale growth, the key factor in promoting MoS<sub>2</sub> in real applications, is still in its early stage. The uniformity in a wafer and wafer-to-wafer is hard to control.

Among the many growth methods, metal–organic chemical vapor deposition (MOCVD) and chemical vapor deposition (CVD) have become the dominant methods to grow MoS<sub>2</sub>.<sup>7–14</sup> In 2015, the Park group reported the growth of MoS<sub>2</sub> wafers by using Mo(CO)<sub>6</sub> and H<sub>2</sub>S as the precursors.<sup>15</sup> Due to the slower growth speed, it takes about one week for 2-inch growth. On the other hand, the normal CVD using evaporated Na<sub>2</sub>MoO<sub>4</sub> has the best advantage of fast growth speed, which can even reach 144 μm min<sup>-1</sup>.<sup>16</sup> However, understanding how to control the uniform distribution of the precursor and further control the uniformity of the as-grown MoS<sub>2</sub> is important. More and more scientists are paying attention to this point. Zhang's group employed pre-oxidized Mo foil to replace MoO<sub>3</sub> or (NH<sub>4</sub>)<sub>2</sub>MoO<sub>4</sub> powder.<sup>17</sup> It was found that MoS<sub>2</sub> can be grown as large as 6 inches. The key factor is controlling the uniformity of the pre-oxidized Mo foil. Apart from this method, although there are many literature studies that report large-scale growth, the methods are still not very good. A breakthrough was achieved by Wang *et al.* through a multi-source CVD configuration enabling a uniform point-source precursor reaction across 4-inch growth substrates.<sup>18</sup> To enhance morphological homogeneity and operational stability in MoS<sub>2</sub> wafer fabrication, researchers developed a face-to-face deposition approach.

College of Materials Science and Engineering, Sichuan University, Chengdu 610065, China. E-mail: zegao@scu.edu.cn

This methodology employs precursor surface diffusion mechanisms through controlled vapor-phase delivery, achieving optimized spatial distribution *via* interfacial energy minimization. Notably, Tang's team engineered a dual-source deposition system by spin-coating S/Se-metal salt composites on molybdenum foil, achieving wafer-scale  $\text{MoS}_{2(1-x)}\text{Se}_{2x}$  monolayers through controlled parallel substrate alignment.<sup>19</sup> Concurrently, Chiu *et al.* demonstrated a stacked CVD approach with constant precursor gradients, realizing synthesis of monolayer  $\text{MoS}_2$  with  $490\text{ cm}^2$  deposition coverage.<sup>20</sup> Despite these advancements, current face-to-face strategies exhibit intrinsic limitations in scalability and process economics, impeding industrial-scale manufacturing of 2D materials. This technological gap necessitates the creation of streamlined synthesis protocols that simultaneously optimize production efficiency, uniformity preservation, and thermodynamic stability. The realization of such synthesis protocols would accelerate the technological maturation of 2D semiconductors for next-generation optoelectronic devices and high-sensitivity sensor arrays.

In this work, we propose a novel face-to-face growth strategy for synthesizing wafer-scale monolayer  $\text{MoS}_2$  on sapphire substrates. The method involves spraying a Mo precursor onto high-temperature-resistant quartz glass, which serves as a surface source. This approach ensures a uniform distribution of the Mo precursor across a carrier substrate with dimensions identical to those of the growth substrate, thereby significantly improving the uniformity and stability of the as-grown  $\text{MoS}_2$ . Systematic investigations were conducted to evaluate the effects of Mo-precursor concentration and spray time on  $\text{MoS}_2$  synthesis. Notably, when monolayer coverage reaches 100%, bilayer coverage exhibits a proportional increase with elevated precursor concentrations or extended spray times. Raman spectra characterization and PL spectra characterization of the as-grown  $\text{MoS}_2$  reveal that bilayer nucleation critically influences the quality. Moreover, excessive bilayer nucleation density results in severe degradation of electrical properties, primarily due to bilayer nuclei acting as scattering centers. This scalable preparation method demonstrates simplicity and cost-effectiveness, enabling the fabrication of highly uniform and stable  $\text{MoS}_2$  films for industrial applications.

## Results and discussion

Since the growth of  $\text{MoS}_2$  in 2010, more and more investigations have focused on how to grow large-scale  $\text{MoS}_2$  films with high uniformity, thus enabling further potential applications in electronics and optoelectronics.<sup>21,22</sup> Many efforts have been made, such as using  $\text{MoO}_3$  and  $(\text{NH}_4)_2\text{MoO}_4$  powder as the precursors, whose vaporization points are very close to the  $\text{MoS}_2$  film growth temperature.<sup>23,24</sup> However, the powder-like source leads to non-uniform evaporation, especially when it is used for large-scale growth. The non-uniform distribution of evaporation makes the  $\text{MoS}_2$  film non-uniform, hindering its further application. Recently, pre-oxidized Mo foil with a

large area was placed face-to-face on a glass substrate.<sup>17</sup> It was found that the as-grown  $\text{MoS}_2$  can enlarge to 6 inches. Our group has also performed this experiment; however, it was found that the  $\text{MoO}_3$  evaporation strongly depends on the state of the pre-oxidized Mo foil. To make the precursor stable and uniform, here, we propose a new method, namely spraying of  $\text{Na}_2\text{MoO}_4$  solution, which can form a highly uniform Mo-precursor layer on 2-inch quartz glass, as shown in Fig. 1a. The uniformly distributed  $\text{Na}_2\text{MoO}_4$  will react with the 2-inch quartz substrate to produce a Na–Mo–Si–O composite and then release a uniform molybdenum source.<sup>25</sup> After reaction with the S vapor released from the ZnS crystal, a uniform  $\text{MoS}_2$  film is formed on the sapphire substrate, and the Zn element is not doped into  $\text{MoS}_2$  (Fig. S1).<sup>26</sup> As shown in Fig. 1b, c and S2a–f, one can see that the  $\text{MoS}_2$  film has similar contrast, indicating its uniformity. The step height in Fig. 1c is about 0.81 nm, which is very close to the intrinsic thickness of monolayer  $\text{MoS}_2$ .<sup>27</sup> The high-resolution HAADF image shown in Fig. 1d exhibits a monolayer sandwich structure, further proving that the as-grown  $\text{MoS}_2$  is a monolayer.<sup>28</sup> To further check the film microstructure, the line scans along the X and Y directions across the whole wafer are shown in Fig. 1e and f. As seen, the positions and intensities of the  $A_{1g}$  and  $E_{2g}$  bands are similar without typical variation, suggesting its high uniformity. PL spectra of the  $\text{MoS}_2$  wafer could also reflect the uniformity in different regions, as shown in Fig. S3a and b. X-ray photoelectron spectroscopy was employed to study the as-grown  $\text{MoS}_2$  film. As shown in Fig. 1g and h, one can see that the signal from 240 eV to 223 eV can be deconvoluted into Mo  $3d_{5/2}$  and Mo  $3d_{3/2}$ ,  $\text{MoS}_x\text{O}_y$  and S 2s. The existence of  $\text{MoS}_x\text{O}_y$  located at about 236.32 eV is caused by surface oxygen adsorption, which is widely observed in the literature.<sup>29,30</sup> The S 2p spectra can be deconvoluted into S  $2p_{1/2}$  and S  $2p_{3/2}$ . By normalizing the Mo and S areas in the XPS spectrum, it was found that the atomic ratio of S/Mo is about 1.89. This indicates the existence of sulfur vacancies.

In order to gain insight into the growth mechanism of Mo-precursor spraying, we first studied the influence of precursor concentration, as shown in Fig. 2. We fixed the spray time as 8 min and tuned the Mo-precursor concentration from  $5\text{ mg mL}^{-1}$  to  $15\text{ mg mL}^{-1}$ . The digital images of  $\text{MoS}_2$  wafers (Fig. 2a–e) show the high coverage of the as-grown  $\text{MoS}_2$  on sapphire. The monolayer coverage is 100% when the concentration of the aqueous solution of  $\text{Na}_2\text{MoO}_4$  is increased in the range from  $7.5\text{ mg mL}^{-1}$  to  $15\text{ mg mL}^{-1}$ . As illustrated in Fig. 2f, when the Mo-precursor concentration is  $5\text{ mg mL}^{-1}$ , the  $\text{MoS}_2$  film is discontinuous, where the monolayer coverage is about 94.32% and no bilayer  $\text{MoS}_2$  is formed. When increasing the Mo-precursor concentration, the coverage of bilayer  $\text{MoS}_2$  increases. The bilayer  $\text{MoS}_2$  coverage is less than 2% when the Mo-precursor concentration is in the range from  $7.5\text{ mg mL}^{-1}$  to  $10\text{ mg mL}^{-1}$ , which means that the  $\text{MoS}_2$  film is a large-area uniform monolayer. The bilayer  $\text{MoS}_2$  coverage can even reach about 10.32% when the precursor concentration is  $15\text{ mg mL}^{-1}$ . Fig. 2g and h show that with the increase of Mo-precursor concentration, the Raman peak position of  $E_{2g}$  red shifts, while the  $A_{1g}$  position does not show

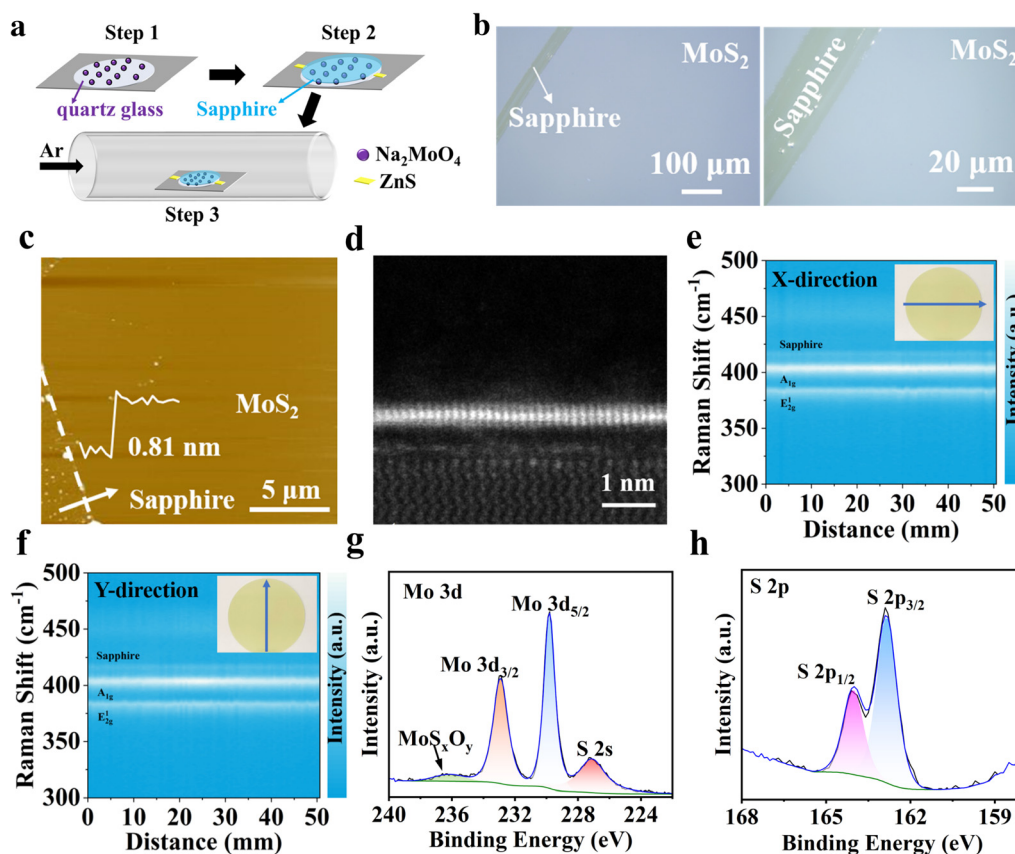


**Fig. 1** The growth of a wafer-scale MoS<sub>2</sub> monolayer. (a) Diagram of the growth process. (b) The optical image of the MoS<sub>2</sub> film on sapphire. (c) The AFM image. (d) The high-resolution HAADF image of the section. (e and f) The Raman spectrum along the X and Y directions across the 2-inch wafer. (g and h) The high-resolution Mo 3d and S 2p spectra.

obvious change. The peak position difference ( $A_{1g}-E_{2g}$ ) is well known to correlate with the thickness of MoS<sub>2</sub>.<sup>31</sup> As seen, with increasing Mo-precursor concentration, the value of  $A_{1g}-E_{2g}$  changes from 17 cm<sup>-1</sup> to 21 cm<sup>-1</sup>, which is well consistent with the evolution of bilayer MoS<sub>2</sub> coverage. The PL spectra are shown in Fig. 2i. It can be seen that when the Mo-precursor concentration is 7.5 mg mL<sup>-1</sup> or 10 mg mL<sup>-1</sup>, the PL peak centers are located at 1.88 eV, which is well consistent with exfoliated MoS<sub>2</sub> single-crystal flakes.<sup>32</sup> However, when the Mo-precursor concentration is less than 7.5 mg mL<sup>-1</sup> or larger than 10 mg mL<sup>-1</sup>, the PL peak centers all redshift suggesting that the optical bandgap becomes lower, which may be caused by the interaction between the bilayer and the monolayer. Statistical analysis of the PL spectra (Fig. S4a) clearly exhibits a sharp decrease of PL intensity and an evident increase of full width at half maxima (FWHM) when increasing the Mo-precursor concentration in the range from 7.5 mg mL<sup>-1</sup> to 15 mg mL<sup>-1</sup>. Combining the Raman vibration analysis and PL emission analysis, one can conclude that the MoS<sub>2</sub> film grown using a 7.5 mg mL<sup>-1</sup> concentration has the highest quality.

Besides the precursor concentration, the spray time is also an important factor, which has been systematically studied as shown in Fig. 3. The Mo-precursor solution is fixed at 7.5 mg

mL<sup>-1</sup>, and the spray time is increased in the range from 7 min to 11 min. As shown in Fig. 3a–e, the growth of monolayer MoS<sub>2</sub> is continuous and has extremely high coverage of 100% when the spray time is more than 7 min. Moreover, the spray time and bilayer coverage are positively correlated, where a longer spray time will lead to higher bilayer coverage. As illustrated in Fig. 3f, the monolayer coverage is 100% and the bilayer coverage is lower than 1% while spraying for 8 min. Raman spectra of MoS<sub>2</sub> with different spray times are shown in Fig. 3g. The statistical analysis of Raman spectra (Fig. 3h) indicates that the peak of  $E_{2g}$  exhibits a redshift and the value of  $A_{1g}-E_{2g}$  changes from 17 cm<sup>-1</sup> to 21 cm<sup>-1</sup> with extending the spray time. The increased bilayer coverage can enhance the interlayer interaction forces between the monolayer and bilayer.<sup>33</sup> PL spectra of MoS<sub>2</sub> with different spray times (Fig. 3i) indicate that their optical bandgap is about 1.8–1.9 eV, well consistent with the nature of monolayer MoS<sub>2</sub>.<sup>34</sup> As illustrated in Fig. S4b, the statistical analysis of the PL spectra demonstrates that the PL intensity rises and FWHM broadens when the spray time is longer than 8 min. Combining the Raman spectra analysis and PL spectra analysis, it can be concluded that the quality of the MoS<sub>2</sub> film is relatively high when the spray time is 8 min and the Mo-precursor concentration is

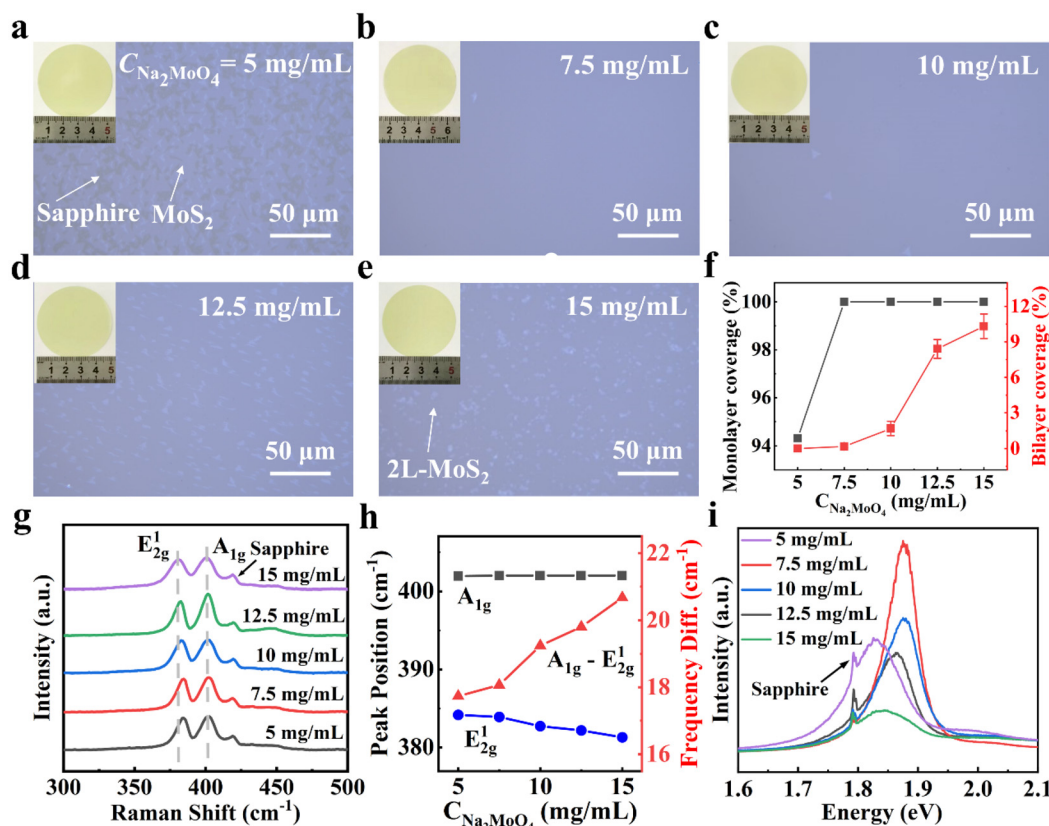


**Fig. 2** The influence of Mo-precursor concentration on MoS<sub>2</sub> growth. (a–e) The digital MoS<sub>2</sub> wafer images and the optical microscopic images with different Mo-precursor concentrations. (f) The monolayer coverage and bilayer coverage as a function of Mo-precursor concentration. (g) Raman spectra of MoS<sub>2</sub> with different Mo-precursor concentrations. (h) The peak positions of E<sub>2g</sub> and A<sub>1g</sub> and the frequency difference of A<sub>1g</sub>–E<sub>2g</sub> as a function of Mo-precursor concentration. (i) PL spectra of MoS<sub>2</sub> with different Mo-precursor concentrations.

7.5 mg mL<sup>-1</sup>. In addition, as shown in Fig. S5 and S6, the growth temperature and environmental pressure have also been studied. It was further determined that 100% monolayer of MoS<sub>2</sub> was obtained at a growth temperature of 820 °C and a pressure of 1 Torr, and there was almost no bilayer nucleation coverage. By this method, we have successfully grown 100 2-inch wafers with a stable process, as illustrated in Fig. S7.

According to the above study, it can be found that with increasing the Mo-precursor concentration and spray time, the bilayer coverage increases while the monolayer coverage reaches 100% on sapphire, which provides a platform to study the optical property evolution from the monolayer to the bilayer. The influence of bilayer coverage on the characterization of Raman and PL spectra is summarized in Fig. 4. As shown in Fig. 4a, the Raman peak position of E<sub>2g</sub> presents a trend of redshift, and the value of A<sub>1g</sub>–E<sub>2g</sub> increases with the bilayer coverage increase. This may be attributed to defects such as sulfur vacancies and lattice dislocations that cause changes in the in-plane lattice stretching state, resulting in a redshift of E<sub>2g</sub> while A<sub>1g</sub> remains unchanged.<sup>35</sup> Furthermore, the increase of bilayer coverage may lead to increased inter-layer interactions, which also contributes to the increase of A<sub>1g</sub>–E<sub>2g</sub>.<sup>33</sup> The PL energy and FWHM as the function of bilayer

coverage are illustrated in Fig. 4b. The FWHM has a negative correlation with bilayer coverage. The PL peak of the direct bandgap red shifts with increasing bilayer coverage, exhibiting that bilayer coverage can change the surface state of the MoS<sub>2</sub> film, affecting the surface electronic state and band structure and leading to the decrease of the direct bandgap peak binding energy.<sup>36</sup> Further pretreatment, such as pre-annealing the sapphire substrate, may improve the surface quality and then suppress bilayer nucleation and bilayer coverage.<sup>37</sup>

To investigate the influence of Mo-precursor spraying on electrical properties of MoS<sub>2</sub> films, transistor arrays were constructed based on MoS<sub>2</sub> films with different Mo-precursor concentrations and spray times, as shown in Fig. 5a. The film is transferred from the growth substrate to a fresh SiO<sub>2</sub>/Si substrate under the assistance of PMMA. In order to remove oxygen and other adsorbed impurities on the surface of the MoS<sub>2</sub> film, the transistor arrays were annealed at 250 °C for two hours under an Ar/H<sub>2</sub> atmosphere. The transfer curves and typical output curves (Fig. 5b, c and Fig. S8–S11) indicate that the MoS<sub>2</sub> film grown by using 10 mg mL<sup>-1</sup> Na<sub>2</sub>MoO<sub>4</sub> solution and spraying for 8 min has the best homogeneity and electric-field effect. The histograms of the carrier mobility and the I<sub>on</sub>/I<sub>off</sub> ratio, as illustrated in Fig. 5d, e and Fig. S12–S14, show that



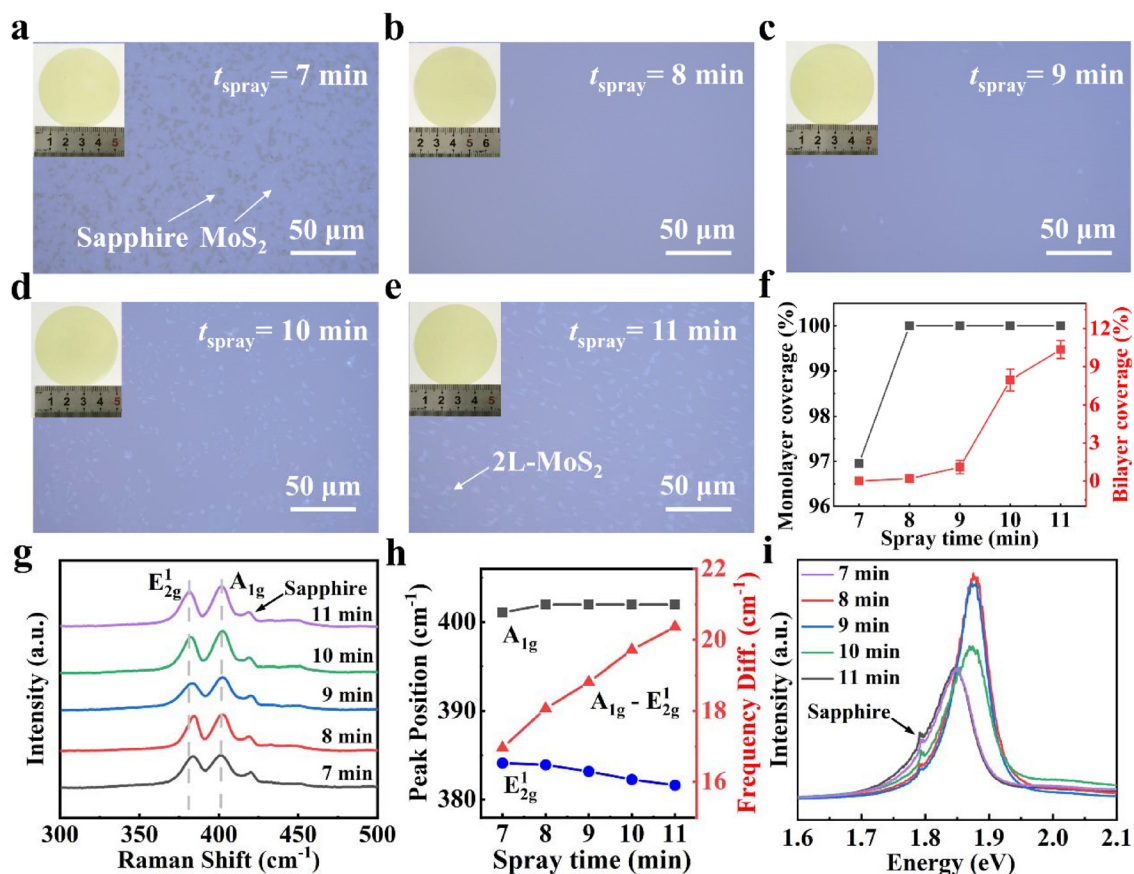


Fig. 3 The influence of spray time on MoS<sub>2</sub> growth. (a–e) The digital MoS<sub>2</sub> wafer images and the optical microscopic images with different spray times. (f) The monolayer coverage and bilayer coverage as a function of spray time. (g) Raman spectra of MoS<sub>2</sub> with different spray times. (h) The peak position of E<sub>2g</sub>, A<sub>1g</sub> and the frequency difference of A<sub>1g</sub>–E<sub>2g</sub> as a function of spray time. (i) PL spectra of MoS<sub>2</sub> with different spray times.

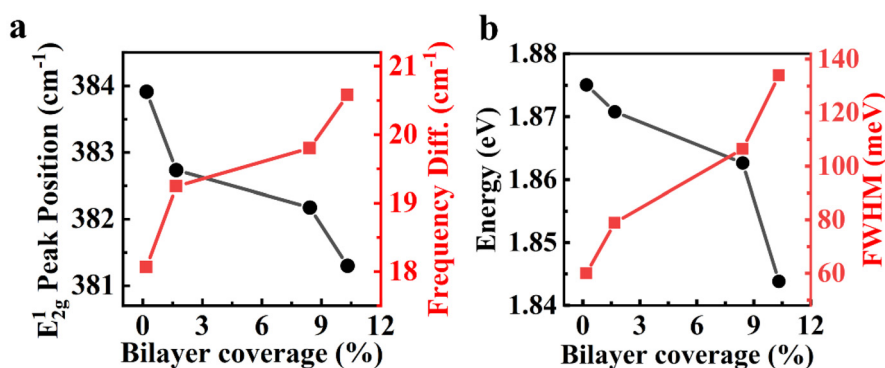
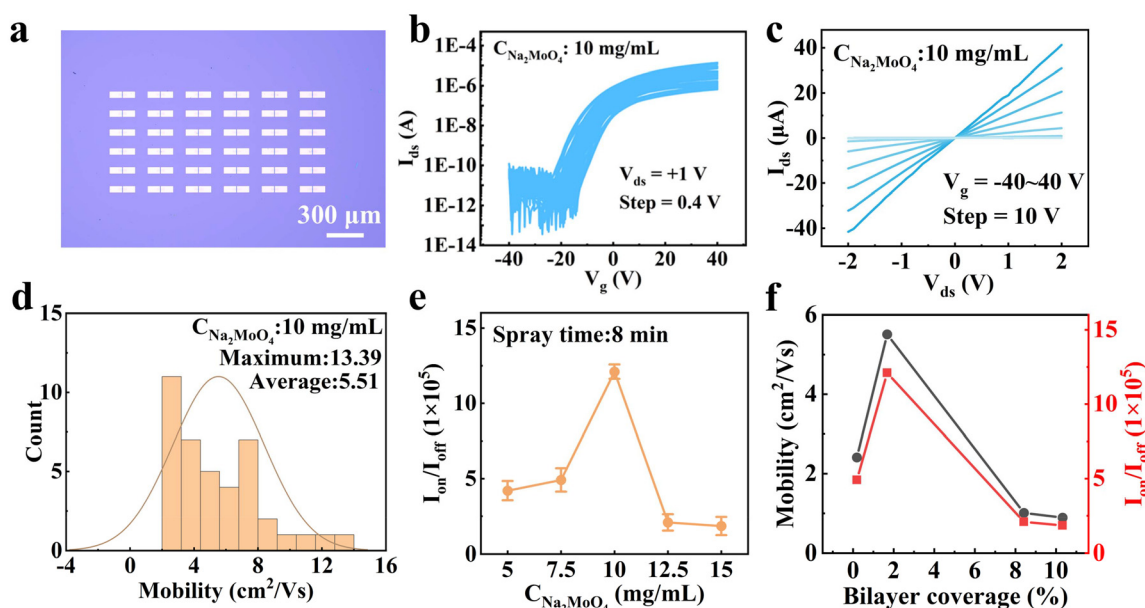


Fig. 4 The influence of bilayer nucleation coverage on the optical properties. (a) The peak position of E<sub>2g</sub> and frequency difference of A<sub>1g</sub>–E<sub>2g</sub> as a function of bilayer coverage. (b) The PL energy as a function of bilayer coverage.

the Mo-precursor concentration and the spray time critically govern the electrical properties of MoS<sub>2</sub> films. Using 10 mg mL<sup>-1</sup> Na<sub>2</sub>MoO<sub>4</sub> aqueous solution and a spray time of 8 min, the MoS<sub>2</sub> carrier mobility can reach 13.39 cm<sup>2</sup> V<sup>-1</sup> s<sup>-1</sup> ( $\mu = g_m \frac{L}{WC_g V_{ds}}$  is used to extract mobility from transfer curves) and the  $I_{on}/I_{off}$  ratio is  $1.21 \times 10^6$ , and the average

values of carrier density, interface trap density and subthreshold swing are  $1.77 \times 10^{12}$  cm<sup>-2</sup>,  $3.46 \times 10^{12}$  eV<sup>-1</sup> cm<sup>-2</sup> and 2.89 V dec<sup>-1</sup>, respectively (Fig. S15). The interface trap density and subthreshold swing of the grown MoS<sub>2</sub> are not much different from the values reported in the literature.<sup>38</sup> It should be noted that carrier mobility is slightly lower compared with the highest value reported in the literature; this should be



**Fig. 5** The electrical properties of the MoS<sub>2</sub> film. (a) The optical image of the transistor array, where the channel length is 5 μm and the channel width is 20 μm. (b) The transfer curves. (c) The typical output curves. (d) The histogram of the carrier mobility where the MoS<sub>2</sub> film is grown by using 10 mg mL<sup>-1</sup> Mo-precursor concentration and spraying for 8 min. (e) The  $I_{\text{on}}/I_{\text{off}}$  ratio as a function of Mo-precursor concentration. (f) The carrier mobility and  $I_{\text{on}}/I_{\text{off}}$  ratio as a function of bilayer coverage.

caused by the contact electrode properties and dielectric surface trapping effects.<sup>39–41</sup> As shown in Fig. S16, the carrier mobility of MoS<sub>2</sub> grown by CVD is consistent with that of mechanically exfoliated MoS<sub>2</sub>, which further indicates the high quality of the film. And the high value of SS in our device is probably attributed to the dielectric interface, such as the surface state and charge traps.<sup>42</sup> Further optimization, including the dielectric interface and contact engineering, will facilitate the improvement of the device performance.<sup>43–45</sup> Furthermore, the carrier mobility and  $I_{\text{on}}/I_{\text{off}}$  ratio as a function of bilayer coverage are plotted in Fig. 5f. It shows that both of these factors show largest values when the bilayer coverage is 1.68%. In our case, lower bilayer coverage may suggest that there are some point defects formed since the Mo precursor is not enough. However, more Mo precursors will lead to bilayer nucleation and cause Fermi fluctuation and grain boundaries, resulting in suppression of the electrical performance.

## Conclusions

In summary, we proposed a new method, Mo-precursor spraying, which can facilitate the growth of highly uniform monolayer MoS<sub>2</sub> wafers. The influence of spraying on MoS<sub>2</sub> preparation was studied by optimizing the Mo-precursor concentration and spray time. This work demonstrates that the Mo-precursor concentration and spray time critically govern the continuity and uniformity of monolayer MoS<sub>2</sub> films, which exhibit a positive correlation with bilayer coverage. Additionally, the effects of bilayer coverage on Raman spectra,

PL spectra and electrical properties of MoS<sub>2</sub> films are studied. As bilayer coverage increases, the Raman peak position of E<sub>2g</sub> red shifts and A<sub>1g</sub>-E<sub>2g</sub> increases. The PL peak position, correlating with the bandgap, shows a trend of redshift and its FWHM becomes broad. Furthermore, high-density and small-sized bilayer nuclei would act as scattering centers, leading to serious deterioration of the electrical properties of the monolayer film. Combining the Raman spectra analysis, PL spectra analysis and electrical measurements, the MoS<sub>2</sub> film grown by using a 10 mg mL<sup>-1</sup> Na<sub>2</sub>MoO<sub>4</sub> solution and spraying for 8 min exhibited relatively high crystal quality. An average  $I_{\text{on}}/I_{\text{off}}$  ratio of  $1.21 \times 10^6$  and a maximum carrier mobility of 13.39 cm<sup>2</sup> V<sup>-1</sup> s<sup>-1</sup> were observed. This simple and cost-effective preparation method provides a general technical means for the wafer-scale growth of 2D materials.

## Experimental section

### CVD growth of MoS<sub>2</sub> monolayer films

The surface of high-temperature resistant quartz glass was spray-coated with 7.5 mg mL<sup>-1</sup> Na<sub>2</sub>MoO<sub>4</sub> aqueous solution for 8 min. The parameters of spraying are as follows: the area of the circular nozzle is 7.07 cm<sup>2</sup>, the distance between the nozzle and the substrate is 8 cm, the velocity of the sprayed jet is about 0.2 mL min<sup>-1</sup>, and the source pressure is 80 kPa. A sandwich structure made of sapphire/ZnS/quartz glass is placed at the center of the tube furnace, and ZnS with a size of 5 mm × 5 mm is inserted into the edge between the sapphire and the quartz glass, which not only provides the active sulfur monomer but also adjusts the distance between the sapphire

and the quartz glass by varying its thickness. 400 sccm Ar was introduced into the tube furnace as the carrier gas. The growth process was then conducted at a growth temperature of 800 °C under a vacuum pumped to 1 Torr for 30 minutes. After the growth was completed, the tube furnace was allowed to cool naturally.

### Characterization methods

The optical images were obtained using SG-9XF. AFM was measured using MultiMode-8, Bruker. Raman and PL spectra were recorded using HORIBA with an excitation wavelength of 532 nm. HAADF was performed using Talos F200X with the aberration-corrected function. XPS was performed on AXIS SUPRA+.

### Device fabrication and measurements

First, the fabrication of MoS<sub>2</sub> transistor arrays commenced with the preparation of source/drain electrodes on a Si/SiO<sub>2</sub> substrate, where a uniform film of the NR9-3000PY negative photoresist was first spin-coated (4000 rpm, 20 s) and pre-baked at 140 °C for 7 min to remove solvent and enhance adhesion. Subsequent patterning was achieved using a contact aligner with a 10 s exposure time, followed by post-exposure baking (140 °C, 7 min) to harden the resist, development in an AZ 400K developer for 45 s to form the template, electron-beam evaporation of a Ti/Au bilayer (10 nm Ti/15 nm Au), and final removal of residual photoresist using acetone and isopropanol. Second, an 8% polymethyl methacrylate solution (PMMA) was spin-coated (4000 rpm, 50 s) onto the MoS<sub>2</sub>-grown sapphire substrate to form a support layer, which was annealed on a hotplate at 180 °C for 3 min to strengthen interfacial adhesion. Leveraging the hydrophobicity contrast between sapphire and PMMA, the MoS<sub>2</sub>/PMMA stack was then completely delaminated *via* a deionized water flotation method and transferred onto the prefabricated source/drain electrodes. After vacuum-drying for 1 h, the PMMA support was dissolved by sequential rinsing in acetone and isopropanol, resulting in an MoS<sub>2</sub> channel layer aligned with the metal electrodes. In the end, to define the channel region, micropatterning was performed using the RZJ-304 positive photoresist: spin-coated (4000 rpm, 20 s), soft-baked on a hotplate (100 °C, 5 min) to ensure uniformity, exposed *via* contact lithography (8 s), developed in an AZ 400K developer for 25 s to form an etch mask, selectively etched using an oxygen plasma system to remove excess MoS<sub>2</sub> while preserving the channel structure with a width of 20 µm and a length of 5 µm, and finally, the photoresist was stripped with acetone, thus completing the MoS<sub>2</sub> transistor array fabrication. The electrical measurements were performed using an LPS-100 vacuum probe station with Keithley 2614 source meters.

### Author contributions

Z. W. conceived, designed and supervised the project. X. L., J. L., D. L., C. Z., X. Z., Z. W. and C. T. conducted the experi-

mental work and performed the data analysis. X. L. and Z. W. wrote the manuscript. All authors contributed to the discussion of the results and editing of the manuscript.

### Conflicts of interest

There are no conflicts to declare.

### Data availability

The data supporting this article have been included as part of the SI.

### Acknowledgements

This work was financially supported by the National Natural Science Foundation of China (52272160 and U2330112), the Sichuan Science and Technology Foundation (2025YFHZ0102, 2023YFSY0002, and 2024JDRC0021), the National Key Research and Development Program of China (2024YFA1209300) and the foundation of Key Laboratory of Lidar and Device, Sichuan Province (Grant No. LLD2023-006).

### References

- 1 K. S. Kim, J. Kwon, H. Ryu, C. Kim, H. Kim, E.-K. Lee, D. Lee, S. Seo, N. M. Han, J. M. Suh, *et al.*, *Nat. Nanotechnol.*, 2024, **19**, 895–906.
- 2 A. Liu, X. Zhang, Z. Liu, Y. Li, X. Peng, X. Li, Y. Qin, C. Hu, Y. Qiu, H. Jiang, *et al.*, *Nano-Micro Lett.*, 2024, **16**, 119.
- 3 M. J. Dai, X. R. Zhang and Q. J. Wang, *Adv. Funct. Mater.*, 2024, **34**, 2312872.
- 4 D. Moon, W. Lee, C. Lim, J. Kim, J. Kim, Y. Jung, H.-Y. Choi, W. S. Choi, H. Kim, J.-H. Baek, *et al.*, *Nature*, 2025, **638**, 957–964.
- 5 I. H. Abidi, S. P. Giridhar, J. O. Tollerud, J. Limb, M. Waqar, A. Mazumder, E. L. H. Mayes, B. J. Murdoch, C. L. Xu, A. Bhoriya, *et al.*, *Adv. Funct. Mater.*, 2024, **34**, 2402402.
- 6 Z. J. Li, H. Bretscher and A. Rao, *Nanoscale*, 2024, **16**, 9728–9741.
- 7 T. S. Kim, K. P. Dhakal, E. Park, G. Noh, H. J. Chai, Y. Kim, S. Oh, M. Kang, J. Park, J. Kim, *et al.*, *Small*, 2022, **18**, 2106368.
- 8 Y. Yang, Y. Y. Qiu, B. Hua, J. L. Cai, Y. L. Zhang, K. C. Cao, X. Q. Shen and Q. Q. Ji, *ACS Mater. Lett.*, 2024, **6**, 2802–2808.
- 9 R. K. Prasad and D. K. Singh, *ACS Omega*, 2023, **8**, 10930–10940.
- 10 A. Fan, Q. Zhang, Z. Ren, L. Li, Z. Han, W. Ma, X. Shen, J. Dong, X. Yu, D. Geng, *et al.*, *ACS Appl. Mater. Interfaces*, 2024, **16**, 59626–59636.

- 11 R. A. Kalt, A. Arcifa, C. Wäckerlin and A. Stemmer, *Nanoscale*, 2023, **15**, 18871–18882.
- 12 S. Li, Y.-C. Lin, X.-Y. Liu, Z. Hu, J. Wu, H. Nakajima, S. Liu, T. Okazaki, W. Chen, T. Minari, Y. Sakuma, K. Tsukagoshi, K. Suenaga, T. Taniguchi and M. Osada, *Nanoscale*, 2019, **11**, 16122–16129.
- 13 S. Li, *iScience*, 2021, **24**, 103229.
- 14 A. Michail, J. Parthenios, D. Anastopoulos, C. Galiotis, M. Christian, L. Ortolani, V. Morandi and K. Papagelis, *2D Mater.*, 2018, **5**, 035035.
- 15 K. Kang, S. Xie, L. Huang, Y. Han, P. Y. Huang, K. F. Mak, C.-J. Kim, D. Muller and J. Park, *Nature*, 2015, **520**, 656–660.
- 16 S. Wang, Y. H. Zhang, D. Y. Zhao, J. Li, H. Kang, S. W. Zhao, T. T. Jin, J. X. Zhang, Z. Y. Xue, Y. Wang, *et al.*, *2D Mater.*, 2022, **9**, 015016.
- 17 P. F. Yang, X. L. Zou, Z. P. Zhang, M. Hong, J. P. Shi, S. L. Chen, J. P. Shu, L. Y. Zhao, S. L. Jiang, X. B. Zhou, *et al.*, *Nat. Commun.*, 2018, **9**, 979.
- 18 Q. Wang, N. Li, J. Tang, J. Zhu, Q. Zhang, Q. Jia, Y. Lu, Z. Wei, H. Yu, Y. Zhao, *et al.*, *Nano Lett.*, 2020, **20**, 7193–7199.
- 19 P. Tang, H. Shu, M. Yang, M. Zhang, C. Sheng, P. Liang, D. Cao and X. Chen, *ACS Appl. Nano Mater.*, 2021, **4**, 12609–12618.
- 20 S.-K. Chiu, X.-Y. Huang, C.-C. Peng, Z.-C. Yang, Y.-Y. Cheng, S.-H. Hu, C.-L. Chiu, C.-W. Chan and S.-H. Chen, *J. Phys. Chem. C*, 2022, **126**, 11201–11208.
- 21 L. Li, Q. Wang, F. Wu, Q. Xu, J. Tian, Z. Huang, Q. Wang, X. Zhao, Q. Zhang, Q. Fan, *et al.*, *Nat. Commun.*, 2024, **15**, 1825.
- 22 J. Zhu, J.-H. Park, S. A. Vitale, W. Ge, G. S. Jung, J. Wang, M. Mohamed, T. Zhang, M. Ashok, M. Xue, *et al.*, *Nat. Nanotechnol.*, 2023, **18**, 456–463.
- 23 W. Li, Q. Qin, X. Li, Y. Huangfu, D. Shen, J. Liu, J. Li, B. Li, R. Wu and X. Duan, *Adv. Mater.*, 2024, **36**, 2408367.
- 24 G. Xue, X. Sui, P. Yin, Z. Zhou, X. Li, Y. Cheng, Q. Guo, S. Zhang, Y. Wen, Y. Zuo, *et al.*, *Sci. Bull.*, 2023, **68**, 1514–1521.
- 25 H. Kim, G. H. Han, S. J. Yun, J. Zhao, D. H. Keum, H. Y. Jeong, T. H. Ly, Y. Jin, J.-H. Park, B. H. Moon, S.-W. Kim and Y. H. Lee, *Nanotechnology*, 2017, **28**, 36LT01.
- 26 Y. Zuo, C. Liu, L. Ding, R. Qiao, J. Tian, C. Liu, Q. Wang, G. Xue, Y. You, Q. Guo, J. Wang, Y. Fu, K. Liu, X. Zhou, H. Hong, M. Wu, X. Lu, R. Yang, G. Zhang, D. Yu, E. Wang, X. Bai, F. Ding and K. Liu, *Nat. Commun.*, 2022, **13**, 1007.
- 27 S. S. Withanage, H. Kalita, H.-S. Chung, T. Roy, Y. Jung and S. I. Khondaker, *ACS Omega*, 2018, **3**, 18943–18949.
- 28 T. Li, W. Guo, L. Ma, W. Li, Z. Yu, Z. Han, S. Gao, L. Liu, D. Fan, Z. Wang, *et al.*, *Nat. Nanotechnol.*, 2021, **16**, 1201–1207.
- 29 X. Zhang, J. Xu, A. Zhi, J. Wang, Y. Wang, W. Zhu, X. Han, X. Tian, X. Bai, B. Sun, *et al.*, *Adv. Sci.*, 2024, **11**, 2408640.
- 30 Y.-Y. Lai, C.-H. Chuang, Y.-W. Yeh, C.-H. Hou, S.-C. Hsu, Y. Chou, Y.-C. Chou, H.-C. Kuo, Y. S. Wu and Y.-J. Cheng, *ACS Appl. Nano Mater.*, 2021, **4**, 4930–4938.
- 31 P. Yang, F. Liu, X. Li, J. Hu, F. Zhou, L. Zhu, Q. Chen, P. Gao and Y. Zhang, *Small Methods*, 2023, **7**, 2300165.
- 32 J. Liu, C. Zhang, Y. Huang, H. Wu, C. Tan and Z. Wang, *Nanoscale*, 2024, **16**, 22403–22410.
- 33 T. S. Kim, G. Noh, S. Kwon, J. Y. Kim, K. P. Dhakal, S. Oh, H. J. Chai, E. Park, I. S. Kim, E. Lee, *et al.*, *Adv. Funct. Mater.*, 2024, **34**, 2312365.
- 34 W. Fu, M. John, T. D. Maddumapatabandi, F. Bussolotti, Y. S. Yau, M. Lin and K. E. Johnson Goh, *ACS Nano*, 2023, **17**, 16348–16368.
- 35 Y. Chen, D. Lu, L. Kong, Q. Tao, L. Ma, L. Liu, Z. Lu, Z. Li, R. Wu, X. Duan, L. Liao and Y. Liu, *ACS Nano*, 2023, **17**, 14954–14962.
- 36 S. Golovynskyi, I. Irfan, M. Bosi, L. Seravalli, O. I. Datsenko, I. Golovynska, B. Li, D. Lin and J. Qu, *Appl. Surf. Sci.*, 2020, **515**, 146033.
- 37 L. Li, Y. Peng, J. Tian, F. Wu, X. Guo, N. Li, W. Yang, D. Shi, L. Du and G. Zhang, *Nano Res.*, 2023, **16**, 12794–12799.
- 38 A. Sebastian, R. Pendurthi, T. H. Choudhury, J. M. Redwing and S. Das, *Nat. Commun.*, 2021, **12**, 693.
- 39 Y. Wang, S. Sarkar, H. Yan and M. Chhowalla, *Nat. Electron.*, 2024, **7**, 638–645.
- 40 H. Jung, M. Kim, Y. Lee, G. B. Sim, H. Gu, S. Hong, S. Lee, J. Lee, D. Lee, T. Zou, *et al.*, *ACS Nano*, 2025, **19**, 6069–6078.
- 41 L. Liu, Y. Chen, L. Chen, B. Xie, G. Li, L. Kong, Q. Tao, Z. Li, X. Yang, Z. Lu, *et al.*, *Nat. Commun.*, 2024, **15**, 165.
- 42 B. Yuan, Z. Chen, Y. Chen, C. Tang, W. Chen, Z. Cheng, C. Zhao, Z. Hou, Q. Zhang, W. Gan, J. Gao, J. Wang, J. Xu, G. Hu, Z. Wu, K. Luo, M. Luo, Y. Zhang, Z. Zhang, S. Xiong, C. Cong, W. Bao, S. Ma, J. Wan, P. Zhou and Y. Lu, *Nat. Commun.*, 2024, **15**, 9038.
- 43 S. Song, K.-H. Kim, R. Keneipp, M. Jung, N. Trainor, C. Chen, J. Zheng, J. M. Redwing, J. Kang, M. Drndic, *et al.*, *ACS Nano*, 2025, **19**, 4452–4461.
- 44 J. Xiao, K. Chen, X. Zhang, X. Liu, H. Yu, L. Gao, M. Hong, L. Gu, Z. Zhang and Y. Zhang, *Small Methods*, 2023, **7**, 2300611.
- 45 J. Huang, Y. Li, X. Yu, Z. Liu, F. Wang, Y. Yue, R. Zhang, R. Dai, K. Yang, H. Liu, *et al.*, *ACS Appl. Mater. Interfaces*, 2024, **16**, 62527–62536.